Geometric nonlinear formulation for curved beams with varying curvature

Keqi Pan,[a)] and Jinyang Liu[b)]
School of Naval Architecture, Ocean and Civil Engineering, Shanghai Jiao Tong University, Shanghai 200240, China

(Received 30 August 2012; accepted 25 September 2012; published online 10 November 2012)

Abstract Based on exact Green strain of spatial curved beam, the nonlinear strain-displacement relation for plane curved beam with varying curvature is derived. Instead of using the previous straight beam elements, curved beam elements are used to approximate the curved beam with varying curvature. Based on virtual work principle, rigid-flexible coupling dynamic equations are obtained. Physical experiments were carried out to capture the large overall motion and the strain of curved beam to verify the present rigid-flexible coupling formulation for curved beam based on curved beam element. Numerical results obtained from simulations were compared with those results from the physical experiments. In order to illustrate the effectiveness of the curved beam element methodology, the simulation results of present curved beam elements are compared with those obtained by previous straight beam elements. The dynamic behavior of a slider-crank mechanism with an initially curved elastic connecting rod is investigated. The advantage of employing generalized-α method is pointed out and the special nonlinear dynamic characteristics of the curved beam are concluded. © *2012 The Chinese Society of Theoretical and Applied Mechanics.* [doi:10.1063/2.1206306]

Keywords curved beam, rigid-flexible coupling dynamics, geometric nonlinear, experiment

Rigid-flexible coupling dynamics of multibody system has been studied for a long time,[1,2] however, not much work has been done on the curved beams with varying curvature. Sugiyama and Suda[1] and Shabana and Maqueda[2] utilized the absolute nodal coordinate formulation for the dynamic analysis of the curved and gradient deficient elements based on the concept of the straight beam element approximation.

Although most of studies adopted the curved beam element to approximate the curved beam,[3,4] they mainly focused on the free vibration and static problems. For the rigid-flexible coupling dynamics research, Park and Kim[5] investigated the dynamic characteristics of a rotating curved beam with a tip mass, however, the radius of the curvature of the curved beam is so large that the curved beam approaches straight beam, therefore the finite element method used in this paper is not persuasive enough. Pan and Liu[6] analyzed the nonlinear dynamic analysis of curved beam, however, the model are limited to the curved beam with constant radius. No further work based on the finite element approach has been reported on the curved beam with variable curvature. Furthermore, the influences of the geometrically nonlinear performances of the curved beam were not investigated. It is necessary to use the geometric nonlinear strain-displacement relationships for dynamic modeling of the planar curved beam by simplification of the exact spatial curved beam theory.[7]

As shown in Fig. 1, an arbitrary undeformed geometry central axis of general curved beam is defined in a reference coordinate system (floating frame). The central-line function of the curved beam before deformation is given by

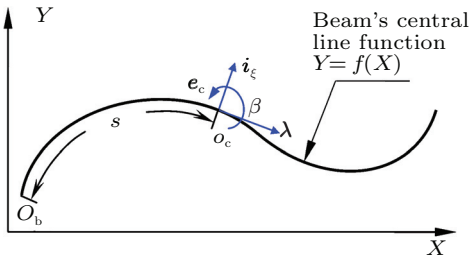

Fig. 1. Axis of the curved beam with varying curvature.

$$Y = f(X). \tag{1}$$

For the general curved beam in Fig. 1, the variant radius of curvature is evaluated as

$$R(X) = [1 + (\mathrm{d}Y/\mathrm{d}X)^2]^{3/2} \left(\mathrm{d}^2Y/\mathrm{d}X^2\right)^{-1}. \tag{2}$$

The displacement fields of an arbitrary point on the curved beam are given as follows

$$\bar{u}(s,\xi,t) = u(s,t) - \xi\beta(s,t), \tag{3}$$

$$\bar{v}(s,\xi,t) = v(s,t), \tag{4}$$

where s represents the arc length along the neutral axis from the left end and ξ is the distance along the thickness direction defined in a local curvilinear frame $\boldsymbol{e}_c$ fixed on an arbitrary point of the neutral axis and β is cross section rotational deformation.

The assumption that the cross section of the beam does not deform in its own plane is introduced. The nonlinear strain components of the planar curved beam

a)Email: keqipan@yahoo.com.cn.
b)Corresponding author. Email: liujy@ sjtu.edu.cn.

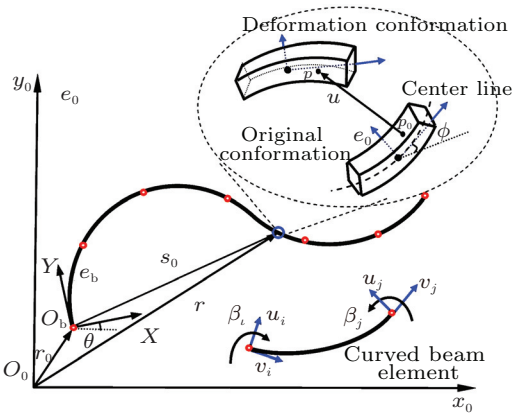

Fig. 2. Configurations of flexible curved beam.

are derived according to Ref. 7 by introducing corresponding plane condition $k_\lambda = k_\xi = 0$, $k_\eta = 1/R$, $\alpha = \gamma = 0$, $\eta = 0$ and small strain assumption $\cos\beta \approx 1$, $\sin\beta \approx \beta$, $g = (1 - \xi k_\eta + \eta k_\xi)^2 \approx 1$. Then the plane curved beam can be obtained as

$$e_{11} = \hat{e}_{11} + \xi k_{11} + \eta k_{22} = (u' - v/R) + \frac{1}{2}u'^2 + \frac{1}{2}v'^2 + \xi k_{11}, \tag{5}$$

$$2e_{12} = \hat{e}_{12} + \eta k_{12} = -\beta + v' + u/R, \tag{6}$$

where $k_{11} = -\beta'$, the superscript prime denotes the derivative with respect to s. The quadratic or higher strain terms in $\hat{e}_{11}$, $\hat{e}_{12}$ and k_{11} are neglected.

The stress-strain relations are given by

$$\sigma_{11} = Ee_{11}, \quad \tau_{12} = G_\xi G 2e_{12}, \tag{7}$$

where E is the modulus of elasticity, G_ξ is the shear modulus and G is the shear coefficient.

The kinematics relations of an arbitrary point on the beam are described with the aid of three coordinate systems as shown in Fig. 2: An inertial frame $\boldsymbol{e}_0$, a floating frame $\boldsymbol{e}_\mathrm{b}$ and a local curvilinear frame $\boldsymbol{e}_\mathrm{c}$.

The coordinate matrix of the displacement of an arbitrary point with respect to $\boldsymbol{e}_0$ can be written as

$$\boldsymbol{r} = \boldsymbol{r}_0 + \boldsymbol{A}_\theta(\boldsymbol{s}_0' + \boldsymbol{A}_\phi \boldsymbol{u}'') = \begin{bmatrix} x_0 \\ y_0 \end{bmatrix} + \boldsymbol{A}_\theta \left(\begin{bmatrix} X \\ Y \end{bmatrix} + \boldsymbol{A}_\phi \begin{bmatrix} \bar{u} \\ \bar{v} \end{bmatrix} \right), \tag{8}$$

where $\boldsymbol{r}_0$ represents the coordinate matrix of $\boldsymbol{r}_0$ defined in $\boldsymbol{e}_0$, $\boldsymbol{s}_0'$ represent the coordinates of $\boldsymbol{s}_0$ defined in $\boldsymbol{e}_\mathrm{b}$, and $\boldsymbol{u}''$ represent the coordinate matrix of deformation vector $\boldsymbol{u}$ of the point p which is defined in frame $\boldsymbol{e}_\mathrm{c}$. $\boldsymbol{A}_\theta$ represents the transformation matrix of frame $\boldsymbol{e}_\mathrm{b}$ with respect to frame $\boldsymbol{e}_0$, and $\boldsymbol{A}_\varphi$ represents the transformation matrix of frame $\boldsymbol{e}_\mathrm{c}$ with respect to frame $\boldsymbol{e}_\mathrm{b}$, which are given by

$$\boldsymbol{A}_\theta = \begin{bmatrix} \cos\theta & -\sin\theta \\ \sin\theta & \cos\theta \end{bmatrix}, \quad \boldsymbol{A}_\phi = \begin{bmatrix} \cos\phi & -\sin\phi \\ \sin\phi & \cos\phi \end{bmatrix}, \tag{9}$$

where $\phi = \tan^{-1}(\mathrm{d}Y/\mathrm{d}X)$ is determined by the initial configure of the curved beam.

The second time-derivative of Eq. (8) is

$$\ddot{\boldsymbol{r}} = \ddot{\boldsymbol{r}}_0 - \boldsymbol{A}_\theta \dot{\theta}^2 (\boldsymbol{s}_0' + \boldsymbol{A}_\phi \boldsymbol{u}'') + \tilde{\boldsymbol{I}} \boldsymbol{A}_\theta \ddot{\theta} (\boldsymbol{s}_0' + \boldsymbol{A}_\phi \boldsymbol{u}'') + 2\tilde{\boldsymbol{I}} \boldsymbol{A}_\theta \dot{\theta} \boldsymbol{A}_\phi \dot{\boldsymbol{u}}'' + \boldsymbol{A}_\theta \boldsymbol{A}_\phi \ddot{\boldsymbol{u}}'', \tag{10}$$

where $\tilde{\boldsymbol{I}}$ represents a skew-symmetric matrix, which can be written as $\tilde{\boldsymbol{I}} = \begin{bmatrix} 0 & -1 \\ 1 & 0 \end{bmatrix}$.

The virtual displacement coordinate vector reads

$$\delta\boldsymbol{r} = \delta\boldsymbol{r}_0 + \tilde{\boldsymbol{I}} \boldsymbol{A}_\theta \delta\theta (\boldsymbol{s}_0' + \boldsymbol{A}_\phi \boldsymbol{u}'') + \boldsymbol{A}_\theta \boldsymbol{A}_\phi \delta\boldsymbol{u}''. \tag{11}$$

In the FEM, the deformations and the Cartesian coordinate for describing the initial shape are interpolated respectively as followings

$$u = \bar{\boldsymbol{N}}_1(\varsigma)\boldsymbol{p}_\mathrm{e}, \; v = \bar{\boldsymbol{N}}_2(\varsigma)\boldsymbol{p}_\mathrm{e}, \; \beta = \bar{\boldsymbol{N}}_3(\varsigma)\boldsymbol{p}_\mathrm{e}, \tag{12}$$

$$\boldsymbol{X}(\varsigma) = \bar{\boldsymbol{N}}(\varsigma)\boldsymbol{X}, \quad \boldsymbol{Y}(\varsigma) = \bar{\boldsymbol{N}}(\varsigma)\boldsymbol{Y}, \tag{13}$$

where ς is the natural coordinate ($-1 \le \varsigma \le 1$), $\bar{\boldsymbol{N}}(\varsigma)$ and $\bar{\boldsymbol{N}}_i(\varsigma)$ $(i = 1, 2, 3)$ are assembled by the isoparametric Lagrange cubic element shape function matrix. $\boldsymbol{p}_\mathrm{e} = (\, u_1^e \;\; v_1^e \;\; \beta_1^e \;\; \cdots \;\; u_4^e \;\; v_4^e \;\; \beta_4^e \,)^\mathrm{T}$ is the generalized coordinate of a curved beam element, which reads $\boldsymbol{p}_\mathrm{e} = \boldsymbol{B}_\mathrm{e}\boldsymbol{p}$, where $\boldsymbol{p}$ is the global elastic coordinate vector. $\boldsymbol{B}_\mathrm{e}$ denotes the Boolean matrix. $\boldsymbol{X}$ and $\boldsymbol{Y}$ represent generalized nodal coordinate value vectors.

On the basis of Eq. (13), the infinitesimal arc element $\mathrm{d}s$ can be expressed as

$$\mathrm{d}s = J_\mathrm{e}(\varsigma)\,\mathrm{d}\varsigma, \tag{14}$$

where $J_\mathrm{e}(\varsigma) = \sqrt{(\mathrm{d}X(\varsigma)/\mathrm{d}\varsigma)^2 + (\mathrm{d}Y(\varsigma)/\mathrm{d}\varsigma)^2}$.

According to Eqs. (10) and (11), the virtual work of the inertia force is expressed as

$$\delta W_i = -\rho \int_V \delta\boldsymbol{r}^\mathrm{T} \ddot{\boldsymbol{r}} \mathrm{d}V = -\delta\boldsymbol{q}^\mathrm{T}\boldsymbol{M}\ddot{\boldsymbol{q}} + \delta\boldsymbol{q}^\mathrm{T}\boldsymbol{Q}_\mathrm{m}, \tag{15}$$

where V represents the volume of the beam and ρ is the mass density, $\boldsymbol{q} = [\boldsymbol{r}_0^\mathrm{T} \;\; \theta \;\; \boldsymbol{p}^\mathrm{T}]^\mathrm{T}$ is the generalized coordinate of the system, and $\boldsymbol{M}$, $\boldsymbol{Q}_\mathrm{m}$ are the generalized mass and inertia force matrices which are given in Appendix.

Considering Eq. (11), the virtual work of the body force can be written as

$$\delta W_\mathrm{F} = \int_V \delta\boldsymbol{r}^\mathrm{T}\boldsymbol{f}\mathrm{d}V = \delta\boldsymbol{q}^\mathrm{T}\boldsymbol{Q}_\mathrm{F}, \tag{16}$$

where $\boldsymbol{f}$ represents the body force vector defined in the inertial frame, and $\boldsymbol{Q}_\mathrm{F}$ represents the generalized body force vector, which is given in Appendix.

According to Eq. (12), Eqs. (5) and (6) can be written as

$$\boldsymbol{\varepsilon} = \boldsymbol{\varepsilon}_\mathrm{L} + \boldsymbol{\varepsilon}_\mathrm{N} + \xi\boldsymbol{\kappa}, \tag{17}$$

where, $\boldsymbol{\varepsilon} = (e_{11} \quad 2e_{12})^{\mathrm{T}}$ and $\boldsymbol{\varepsilon}_{\mathrm{L}} = \boldsymbol{B}_{\mathrm{L0}}\boldsymbol{p}_{\mathrm{e}}$ denote the linear strain component, $\boldsymbol{\kappa} = \boldsymbol{B}_{\mathrm{L}\kappa}\boldsymbol{p}_{\mathrm{e}}$ represents curvatures, and $\boldsymbol{\varepsilon}_{\mathrm{N}} = \boldsymbol{C}\boldsymbol{\Theta}/2$ is the nonlinear strains. $\boldsymbol{B}_{\mathrm{L0}}$, $\boldsymbol{B}_{\mathrm{L}\kappa}$, $\boldsymbol{C}$ and $\boldsymbol{\Theta}$ are given by

$$\boldsymbol{B}_{\mathrm{L0}} = \begin{bmatrix} \bar{\boldsymbol{N}}'_1 - \bar{\boldsymbol{N}}_2/R \\ \bar{\boldsymbol{N}}'_2 + \bar{\boldsymbol{N}}_1/R - \bar{\boldsymbol{N}}_3 \end{bmatrix},$$

$$\boldsymbol{B}_{\mathrm{L}\kappa} = \begin{pmatrix} \bar{\boldsymbol{N}}'_3 \\ \boldsymbol{0} \end{pmatrix}, \tag{18}$$

$$\boldsymbol{C} = \begin{bmatrix} \bar{\boldsymbol{N}}'_1\boldsymbol{p}_{\mathrm{e}} & \bar{\boldsymbol{N}}'_2\boldsymbol{p}_{\mathrm{e}} \\ 0 & 0 \end{bmatrix},$$

$$\boldsymbol{\Theta} = \boldsymbol{G}\boldsymbol{p}_{\mathrm{e}} = \begin{bmatrix} \bar{\boldsymbol{N}}'_1 \\ \bar{\boldsymbol{N}}'_2 \end{bmatrix} \boldsymbol{p}_{\mathrm{e}}, \tag{19}$$

where $\bar{\boldsymbol{N}}'_i = \dfrac{1}{J_e(\zeta)} \dfrac{\mathrm{d}\bar{\boldsymbol{N}}_i}{\mathrm{d}\zeta} \quad i = 1, 2, 3.$

Since $\delta\boldsymbol{C}\boldsymbol{\Theta} = \boldsymbol{C}\delta\boldsymbol{\Theta}$, according to Eqs. (17)–(19), the variation of the Green strain can be written as

$$\delta\boldsymbol{\varepsilon} = (\boldsymbol{B}_{\mathrm{L0}} + \boldsymbol{C}\,\boldsymbol{G})\,\delta\boldsymbol{p}_{\mathrm{e}} + \xi\boldsymbol{B}_{\mathrm{L}\kappa}\delta\boldsymbol{p}_{\mathrm{e}}. \tag{20}$$

Considering Eqs. (17) and (20), the virtual work of the internal force considering geometric nonlinear effect can be written as

$$\delta W_{\mathrm{in}} = -\int_V \delta\boldsymbol{\varepsilon}\boldsymbol{D}\boldsymbol{\varepsilon}\mathrm{d}V = \delta\boldsymbol{q}^{\mathrm{T}}\boldsymbol{Q}_{\mathrm{s}} = \delta\,\boldsymbol{q}^{\mathrm{T}}[0 \quad \boldsymbol{f}_{\mathrm{s}}^{\mathrm{T}}]^{\mathrm{T}}, \tag{21}$$

where

$$\boldsymbol{f}_{\mathrm{s}} = -\sum_{e=1}^{N_{\mathrm{e}}} \boldsymbol{B}_{\mathrm{e}}^{\mathrm{T}} \Bigg\{ \int_{-1}^{1} \Bigg[A\,(\boldsymbol{B}_{\mathrm{L0}} + \boldsymbol{C}\,\boldsymbol{G})^{\mathrm{T}} \cdot \boldsymbol{D}\left(\boldsymbol{B}_{\mathrm{L0}} + \frac{1}{2}\boldsymbol{C}\,\boldsymbol{G}\right)\boldsymbol{p}_{\mathrm{e}} + I\boldsymbol{B}_{\mathrm{L}\kappa}^{\mathrm{T}}\boldsymbol{D}\boldsymbol{B}_{\mathrm{L}\kappa}\boldsymbol{p}_{\mathrm{e}} \Bigg] \Bigg\} \mathrm{d}\zeta, \tag{22}$$

$\boldsymbol{D} = \begin{bmatrix} E & 0 \\ 0 & \boldsymbol{G}\boldsymbol{G}_{\xi} \end{bmatrix}$, and A and I are area and inertia moment of curved beam cross section, respectively. If terms $\boldsymbol{C}$ and $\boldsymbol{G}$ are ignored in the Eq. (22), the linear model can be obtained.

According to the principle of virtual work, the sum of Eqs. (15), (16) and (21) leads to

$$\delta W_i + \delta W_{\mathrm{F}} + \delta W_{\mathrm{in}} = \delta\boldsymbol{q}^{\mathrm{T}}\left(-\boldsymbol{M}\ddot{q} + \boldsymbol{Q}_{\mathrm{m}} + \boldsymbol{Q}_{\mathrm{F}} + \boldsymbol{Q}_{\mathrm{s}}\right) = 0. \tag{23}$$

Considering constraints in systems and Eq. (23), the constrained multi-body system equations of motion are given by

$$\begin{bmatrix} \boldsymbol{M} & \boldsymbol{\Phi}\boldsymbol{q}^{\mathrm{T}} \\ \boldsymbol{\Phi}\boldsymbol{q} & \boldsymbol{0} \end{bmatrix} \begin{bmatrix} \ddot{\boldsymbol{q}} \\ \boldsymbol{\lambda} \end{bmatrix} = \begin{bmatrix} \boldsymbol{Q} \\ \boldsymbol{\gamma} \end{bmatrix}, \tag{24}$$

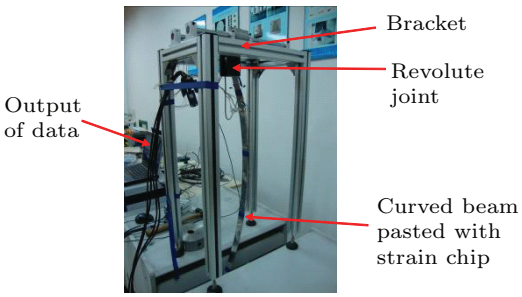

Fig. 3. Photograph of the experiment apparatus.

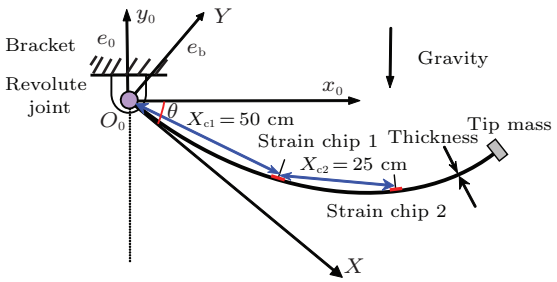

Fig. 4. Curved beam pendulum with tip mass.

where $\boldsymbol{Q} = \boldsymbol{Q}_{\mathrm{m}} + \boldsymbol{Q}_{\mathrm{F}} + \boldsymbol{Q}_{\mathrm{s}}$ and λ represents the matrix of Lagrange multipliers. Dynamic Eq. (24) is integrated by generalized-α method which is given by Ref. 8.

The dynamics of a curved beam pendulum with a tip mass which is linked with the bracket using a revolute joint is studied in experiment, which can be seen in Figs. 3 and 4. The strain chips are pasted on the curved beam, the position of which can be found in Fig. 4, and the strain data can be obtained by those strain chips. The angular velocity of pendulum is measured by the floating frame and the inertial frame which can be seen in Fig. 4. The properties of curved beam with rectangular cross section and initial condition are shown in Table 1.

In order to keep present simulating conditions consistent with those of experiment, the damping forces[9] are considered in the simulating model. Figures 5(a)

Table 1. Experiment parameter.

Parameter	Parameter values
Arc length/m	0.80
Width/m	0.03
Thickness/m	0.002 5
Density/(kg · m^{-3})	2 760.0
Poisson's ratio	0.3
Elastic modulus/GPa	68.950
Radius of curved beam/m	0.85
θ/rad	–0.60
Tip mass/kg	0.060

and 5(b) show the comparison of the strain results obtained from experiment and present simulating model. It can be seen in Figs. 5(a) and 5(b) that the results obtained by nonlinear model are in good agreement with those obtained by experiment, however, there are significant differences between the results obtained by linear simulating model and experiments. The reason is that terms $\boldsymbol{C}$ and $\boldsymbol{G}$ related to nonlinear strain are ignored in the linear model, therefore the accuracy of the model can not be guaranteed. Figure 5(c) compares the results of the angular velocity of the curved beam. As can be seen in Fig. 5(c), the results of measurement and those of linear and nonlinear simulating model agree well, which indicates that the influence of nonlinear related terms $\boldsymbol{C}$ and $\boldsymbol{G}$ on the angular velocity is not obvious for the present experiment case.

The circular and parabolic shaped curved beams are both used in simulation examples.

The equation for the circular shaped curved beam with the constant radius R is defined in floating frame as

$$y = R - \sqrt{R^2 - x^2}, \quad 0 < x < R\sin\alpha, \tag{25}$$

where α is the subtended angle.

The equation for the parabolic shaped curved beam with the non constant radius in floating frame is defined as

$$y = -4dl^2 x\,(x - l)\,, \quad 0 < x < l. \tag{26}$$

The properties of the beam are given as follows: the mass density $\rho = 27\,667\ \mathrm{kg/m^3}$, the modulus of elasticity $E = 68.952$ GPa, the cross-section area $A = 8 \times 10^{-5}\ \mathrm{m^2}$, and the moment of inertia $I = 1.066\,67 \times 10^{-8}\ \mathrm{m^2}$. The curved beam is attached to a rotating rigid hub with radius $R_\mathrm{h} = 0.05$ m and the rotary inertia $J_\mathrm{h} = 0.3\ \mathrm{kg/m}$ respectively. The length of the beams are equal to 5/3 m, and the corresponding subtended angles are $\alpha = 30°$ and $\alpha = 60°$, respectively. The following torque drives the hub in the numerical analysis

$$T = 10\sin(\omega_0 t)\ \ \mathrm{N\cdot m} \quad 0 \le t \le 2\ \mathrm{s}, \tag{27}$$

where $\omega_0 = 2\pi$ rad/s.

The dynamic results of present nonlinear curved beam model are compared with those obtained by the straight beam elements. All the deformations are measured in the inertial coordinate system. The time histories of the tip deformation of the curved beam with $\alpha = 60°$ are shown in Figs. 6 and 7, respectively. It can be seen in Fig. 6 that the longitudinal deformation results obtained by straight beam elements and the results obtained by present nonlinear curved beam element model are in good agreement, and the transverse deformation results in Fig. 7 also coincide well, which verify the correctness of present curved beam elements and straight beam elements.

Although present curved beam and straight beam elements have the same simulation results, as shown in

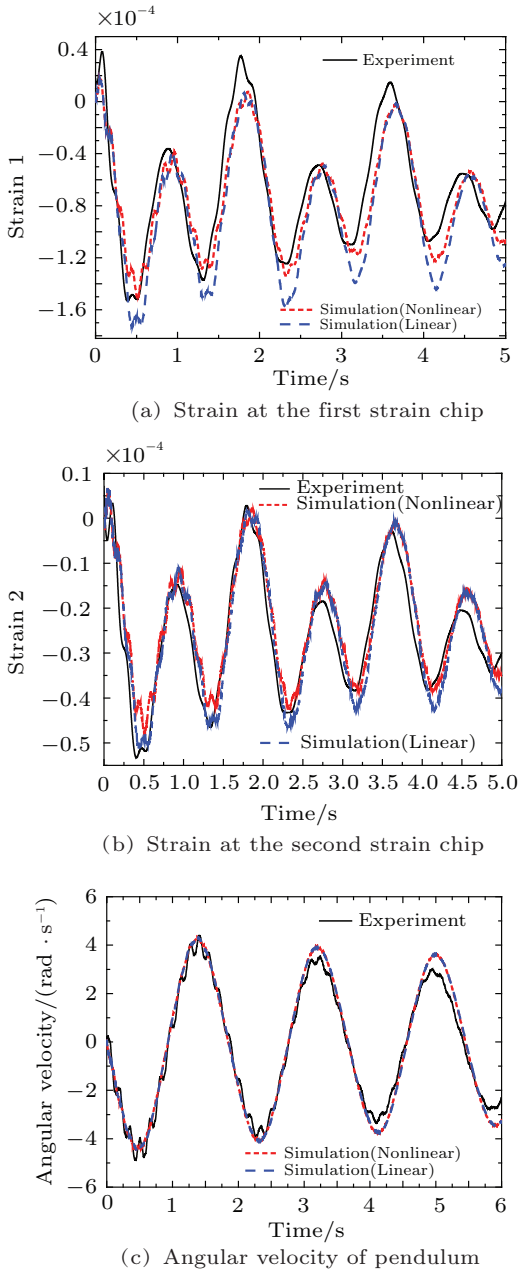

(a) Strain at the first strain chip

(b) Strain at the second strain chip

(c) Angular velocity of pendulum

Fig. 5. Comparison of simulation results with those of experiment.

Table 2, for curved beam with 30° and 60°, the convergence results can be obtained just using at most 4 and 6 curved finite elements for present model, respectively; however, at least 15 and 20 finite elements are needed to converge for the straight beam elements. Furthermore, as can be seen, for the cases of the same length of the curved beams, the curved beam with larger curvature (60°) needs more elements to converge. Table 2 compares the CPU time cost of the present curved beam elements and straight beam approximation elements with time step 0.001 s and end time 2 s. It can be seen that, for the present curved beam element, 6 s and 12 s are cost for simulating the curved beam with 30° and 60°

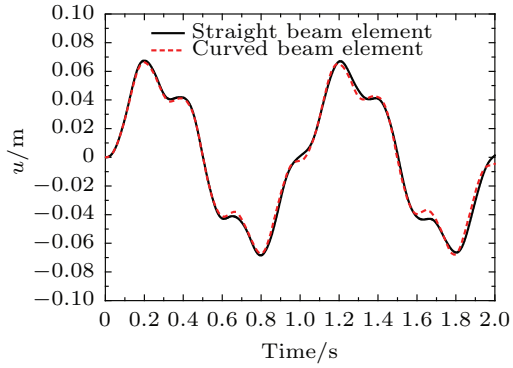

Fig. 6. The tip longitudinal deformation of the curved beam.

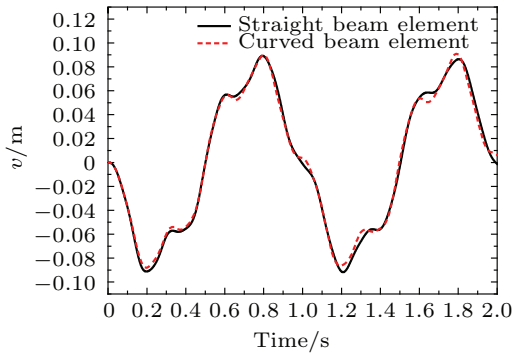

Fig. 7. The tip transverse deformation of the curved beam.

subtended angle respectively, nevertheless, for straight beam approximation elements, the corresponding simulation time are 70 s and 80 s, respectively.

A slider-crank mechanism is shown in Fig. 8. The length of crank is 1 m, square cross-section areas of the crank and the connecting rod are both given by $A = (0.02 \times 0.02)\ \mathrm{m}^2$. The mass of the slider is 0.5 kg. The crank is subjected to a prescribed rotational motion defined by

$$\theta(t) = \begin{cases} \dfrac{\omega_0}{t_\mathrm{s}} \left\{ \dfrac{t^2}{2} + \left(\dfrac{t_\mathrm{s}}{2\pi} \right)^2 \left[\cos\left(\dfrac{2\pi t}{t_\mathrm{s}} \right) - 1 \right] \right\}, \\ \qquad (0 \le t \le t_\mathrm{s}), \\ \omega_0 \left(t - \dfrac{t_\mathrm{s}}{2} \right), \\ \qquad (t_\mathrm{s} < t \le t_\mathrm{m}), \end{cases} \tag{28}$$

Table 2. Time cost and element numbers comparison.

α	Element number		CPU Time/s	
	Curved	Straight	Curved	Straight
30°	4	15	6	70
60°	8	20	12	80

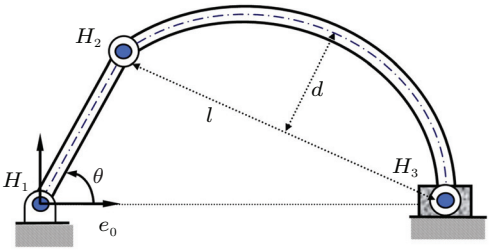

Fig. 8. Slider-crank with flexible connecting rod.

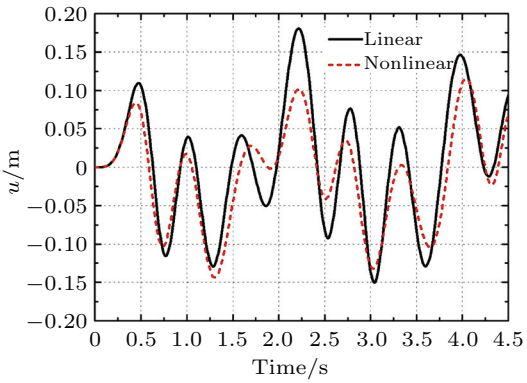

Fig. 9. The longitudinal deformation of the middle point.

where $\omega_0 = \pi$ is the angular velocity of crank at the steady-state stage, and $t_\mathrm{s} = 0.5$ s is the accelerating time.

Figure 9 shows the linear and nonlinear dynamic response of the mechanism with the curved connecting rod of $d = 1$ m, $l = 4$ m. The deformations are measured in the local coordinate system. It is shown that at the initial phase 0–0.35 s the linear and nonlinear results coincide. With the increase of the angular velocity of the crank the vibration amplitude of the longitudinal deformation of the middle point obtained by linear model is becoming larger than that obtained by nonlinear model, which can not explain the dynamic stiffening phenomenon. Influenced by elastic deformation, obvious differences of angular velocity of the connecting rod

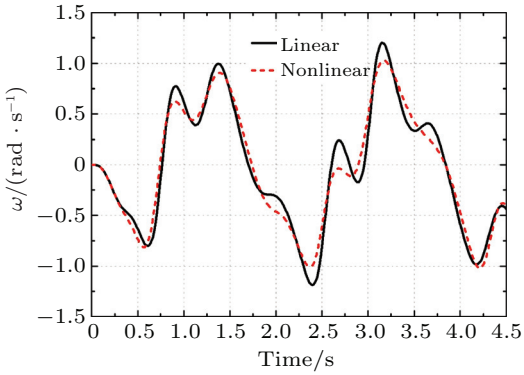

Fig. 10. The angular velocity of the connecting rod.

can be found in Fig. 10.

Nonlinear strain-displacement relations for the plane curved beam with varying curvature are obtained and the nonlinear dynamic equations for the curved beam multi-body systems are established. By physical experiments, the accuracy of present nonlinear rigid-flexible coupling formulation for curved beam with varying curvature is verified. Moreover, due to the neglect of the nonlinear terms in linear model, obvious differences can be found between the results obtained by linear model and those obtained by experiment. Present curved beam element is more efficient than the straight beam element. Considering geometric nonlinear effect is necessary in case of high rotating speed.

APPENDIX

$$\boldsymbol{M}=\begin{bmatrix}\boldsymbol{M}_{rr} & \boldsymbol{M}_{r\theta} & \boldsymbol{M}_{rp}\\ \boldsymbol{M}_{\theta r} & M_{\theta\theta} & \boldsymbol{M}_{\theta p}\\ \boldsymbol{M}_{p\theta} & \boldsymbol{M}_{p\theta} & \boldsymbol{M}_{pp}\end{bmatrix},$$

$$\boldsymbol{Q}_{\mathrm{m}}=\begin{bmatrix}\boldsymbol{Q}_r\\ \boldsymbol{Q}_\theta\\ \boldsymbol{Q}_p\end{bmatrix},$$

$$\boldsymbol{Q}_{\mathrm{F}}=\begin{bmatrix}\boldsymbol{f}_r\\ \boldsymbol{f}_\theta\\ \boldsymbol{f}_p\end{bmatrix}, \tag{29}$$

where

$$\boldsymbol{M}_{rr}=m\begin{bmatrix}1 & 0\\ 0 & 1\end{bmatrix},$$

$$\boldsymbol{M}_{r\theta}=\rho\,A\tilde{\boldsymbol{I}}\,\boldsymbol{A}_\theta\sum_{e=1}^{N_{\mathrm{e}}}\int_{-1}^{1}\left(\boldsymbol{s}_0'+\boldsymbol{A}_\phi\boldsymbol{N}\boldsymbol{p}\right)J_{\mathrm{e}}\left(\varsigma\right)\mathrm{d}\varsigma,$$

$$\boldsymbol{M}_{rp}=\rho A\boldsymbol{A}_\theta\sum_{e=1}^{N_{\mathrm{e}}}\int_{-1}^{1}\boldsymbol{A}_\phi\boldsymbol{N}J_{\mathrm{e}}(\varsigma)\mathrm{d}\varsigma,$$

$$\boldsymbol{M}_{\theta\theta}=\rho\sum_{e=1}^{N_{\mathrm{e}}}\int_{-1}^{1}\Big[A\left(\boldsymbol{s}_0'+\boldsymbol{A}_\phi\boldsymbol{N}\boldsymbol{p}\right)^{\mathrm{T}}\left(\boldsymbol{s}_0'+\boldsymbol{A}_\phi\boldsymbol{N}\boldsymbol{p}\right)+ I\boldsymbol{p}^{\mathrm{T}}\boldsymbol{N}_I^{\mathrm{T}}\boldsymbol{N}_I\boldsymbol{p}\Big]J_{\mathrm{e}}\left(\varsigma\right)\mathrm{d}\varsigma,$$

$$\boldsymbol{M}_{\theta p}=\rho\sum_{e=1}^{N_{\mathrm{e}}}\int_{-1}^{1}\Big[A\left(\boldsymbol{s}_0'+\boldsymbol{A}_\phi\boldsymbol{N}\boldsymbol{p}\right)^{\mathrm{T}}\tilde{\boldsymbol{I}}^{\mathrm{T}}\boldsymbol{A}_\phi\boldsymbol{N}+ I\boldsymbol{p}^{\mathrm{T}}\boldsymbol{N}_I^{\mathrm{T}}\tilde{\boldsymbol{I}}^{\mathrm{T}}\boldsymbol{N}_I\Big]J_{\mathrm{e}}\left(\varsigma\right)\mathrm{d}\varsigma,$$

$$\boldsymbol{M}_{pp}=\rho\sum_{e=1}^{N_{\mathrm{e}}}\int_{-1}^{1}\left(A\boldsymbol{N}^{\mathrm{T}}\boldsymbol{N}+I\bar{\boldsymbol{N}}_I^{\mathrm{T}}\bar{\boldsymbol{N}}_I\right)J_{\mathrm{e}}\left(\varsigma\right)\mathrm{d}\varsigma,$$

$$\boldsymbol{Q}_r=\rho\sum_{e=1}^{N_{\mathrm{e}}}\int_{-1}^{1}\Big[\boldsymbol{A}_\theta\,\dot\theta^2\left(\boldsymbol{s}_0'+\boldsymbol{A}_\phi\boldsymbol{N}\boldsymbol{p}\right)- 2\,\tilde{\boldsymbol{I}}\,\boldsymbol{A}_\theta\,\dot\theta\boldsymbol{A}_\phi\boldsymbol{N}\dot{\boldsymbol{p}}\Big]J_{\mathrm{e}}\left(\varsigma\right)\mathrm{d}\varsigma,$$

$$\boldsymbol{Q}_\theta=-2\rho\dot\theta\sum_{e=1}^{N_{\mathrm{e}}}\int_{-1}^{1}\Big[A\boldsymbol{s}_0'^{\mathrm{T}}\boldsymbol{A}_\phi\boldsymbol{N}+ \boldsymbol{p}^{\mathrm{T}}\left(A\boldsymbol{N}^{\mathrm{T}}\boldsymbol{N}+I\bar{\boldsymbol{N}}_I^{\mathrm{T}}\bar{\boldsymbol{N}}_I\right)\Big]\dot{\boldsymbol{p}}J_{\mathrm{e}}\left(\varsigma\right)\mathrm{d}\varsigma,$$

$$\boldsymbol{Q}_p=\rho\sum_{e=1}^{N_{\mathrm{e}}}\int_{-1}^{1}\Big\{\dot\theta^2\Big[\boldsymbol{N}^{\mathrm{T}}\boldsymbol{A}_\phi^{\mathrm{T}}\boldsymbol{s}_0'+ \left(A\boldsymbol{N}^{\mathrm{T}}\boldsymbol{N}+I\bar{\boldsymbol{N}}_I^{\mathrm{T}}\bar{\boldsymbol{N}}_I\right)\boldsymbol{p}\Big]-2\dot\theta\boldsymbol{N}^{\mathrm{T}}\tilde{\boldsymbol{I}}\,\boldsymbol{N}\dot{\boldsymbol{p}}\Big\}J_{\mathrm{e}}\left(\varsigma\right)\mathrm{d}\varsigma,$$

$$\boldsymbol{f}_r=AL_{\mathrm{s}}\boldsymbol{f},$$

$$\boldsymbol{f}_\theta=\sum_{e=1}^{N_{\mathrm{e}}}\int_{-1}^{1}\Big[\left(\boldsymbol{s}_0'+\boldsymbol{A}_\phi\boldsymbol{N}\boldsymbol{p}\right)^{\mathrm{T}}\boldsymbol{A}_\theta^{\mathrm{T}}\tilde{\boldsymbol{I}}^{\mathrm{T}}\boldsymbol{f}\Big]J_{\mathrm{e}}\left(\varsigma\right)\mathrm{d}\varsigma,$$

$$\boldsymbol{f}_p=\sum_{e=1}^{N_{\mathrm{e}}}\int_{-1}^{1}\left(\boldsymbol{N}^{\mathrm{T}}\boldsymbol{A}_\phi^{\mathrm{T}}\boldsymbol{A}_\theta^{\mathrm{T}}\boldsymbol{f}\right)J_{\mathrm{e}}\left(\varsigma\right)\mathrm{d}\varsigma,$$

where m is the mass of curved beam, $\boldsymbol{N}=\begin{bmatrix}\bar{\boldsymbol{N}}_1\boldsymbol{B}_{\mathrm{e}}\\ \bar{\boldsymbol{N}}_2\boldsymbol{B}_{\mathrm{e}}\end{bmatrix}$, $\boldsymbol{N}_I=\begin{bmatrix}\bar{\boldsymbol{N}}_3\boldsymbol{B}_{\mathrm{e}}\\ 0\end{bmatrix}$, L_{s} is the arch length of curved beam, A is the area of the cross section, N_e is the total number of curved beam elements.

This work was supported by the Research Fund for the Doctoral Program of Higher Education of China (20100073110007) and the Key Project of National Natural Science Foundation of China (11132007).

1. H. Sugiyama, and Y. Suda, J. Multi-body Dyn. **221**, 219 (2007).
2. A. A. Shabana, and L. G. Maqueda, Multibody Syst. Dyn. **20**, 239 (2008).
3. P. Raveendranath, G. Singh, and G. V. Rao, Int. J. Numer. Meth. Eng. **51**, 85 (2001).
4. J. S. Wu, and L. K. Chiang, Int. J. Numer. Meth. Eng. **58**, 1907 (2003).
5. J. H. Park, and J. H. Kim, J. Sound Vib. **228**, 1017 (1999).
6. K. Q. Pan, and J. Y. Liu, Acta Mech. Sin. **27**, 1023 (2011).
7. O. A. Bauchau, and C. H. Hong, AIAA 1469 (1987).
8. A. Martin, and B. Olivier, Multibody Syst. Dyn. **18**, 185 (2007).
9. J. W. Lee, H. W. Kim, and H. C. Ku, J. Sound Vib. **325**, 722 (2009).